Journal of Aerosol Science 79 (2015) 72–85

Contents lists available at ScienceDirect

Journal of Aerosol Science

journal homepage: www.elsevier.com/locate/jaerosci

Estimation of carbon nanotubes deposition in a human respiratory tract replica

Wei-Chung Su *, Yung Sung Cheng

Lovelace Respiratory Research Institute, 2425 Ridgecrest Dr. SE, Albuquerque, NM 87108, USA

ARTICLE INFO

Article history:
Received 20 August 2014
Received in revised form
27 September 2014
Accepted 27 September 2014
Available online 18 October 2014

Keywords:
Carbon nanotubes
Human airway replica
Lung deposition
Deposition efficiency

ABSTRACT

Investigation of the deposition of airborne carbon nanotubes (CNTs) in the human respiratory tract is essential from the occupational health perspective. Due to the dimension of CNTs, it is very difficult to apply traditional deposition experimental methods to CNTs for conducting a deposition study using human airway replicas. In this research, an innovative experimental approach was adopted to estimate the deposition of CNTs in the human respiratory tract. Two types of CNT materials were used as the challenge CNT materials. The deposition experiments were carried out by delivering size classified CNT aerosols into a human airway replica (from the oral cavity down to part of the 4th lung generation). The CNT deposition fractions and efficiencies in the airways were estimated based on the air flow rates, as well as the CNT concentrations measured in associated lung airways. Experimental results acquired showed that CNT deposition fractions in different sections of the airway replica were all smaller than 5%. The CNT deposition efficiency in the tracheobronchial airways was generally less than 0.1. This result implies that the CNTs inhaled into the human respiratory tract could easily penetrate through the upper airways and transit down to the lower airways to cause potential health effects.

1. Introduction

Carbon nanotubes (CNTs) are rolled graphene sheets with a cylindrical nanostructure. The tube diameter of the CNTs ranges from a couple of nanometers to tens of nanometers depending on the number of rolled layers. However, the tube length of the CNTs could be one million times longer than its tube diameter, which results in an extremely large length-to-diameter aspect ratio as the distinctive characteristic for CNTs. CNTs are considered nanomaterials because the tube diameters of CNTs are generally less than 100 nm, which meets the conventional criteria for nanomaterials (material of which at least one external dimension is in the scale less than or equal to 100 nm). Many types of CNTs have been developed and manufactured based on the tube structure of the CNTs. For example, single-walled carbon nanotubes (SWCNTs), multi-walled carbon nanotubes (MWCNTs), and stacked-cup carbon nanotubes (SCCNTs) are all available on the market. Because of their special physical properties in terms of mechanical strength, thermal conductivity, electrical property, and optical property, CNTs have been applied in various state-of-the-art products such as coating materials, batteries, computer memories, and solar cells (Endo et al., 2008). According to published reports, the annual production capacity of CNTs

* Corresponding author. Tel.: +1 505 348 9571; fax: +1 505 348 8567.
E-mail address: wsu@LRRI.org (W.-C. Su).

http://dx.doi.org/10.1016/j.jaerosci.2014.09.005
0021-8502/

worldwide in 2011 had reached 4.6 kt/year (De Volder et al., 2013). By 2015, the total production value of CNTs is expected to be 1.3 billion U.S. dollars globally (Parish, 2011).

Despite the valuable applications of CNTs in some high technology products, the potential health risk of CNTs has rapidly become a serious concern. Workers in CNT associated factories might be exposed to aerosolized CNTs since CNT materials could become airborne involuntarily during manufacturing, application, and cleaning processes (Dahm et al., 2012; Chen et al., 2012). Inhalation and deposition of CNT aerosols in the respiratory tract could cause possible adverse biological responses in the worker's lung. Based on CNT animal exposure studies summarized in the recent NIOSH report (NIOSH, 2013), exposure to CNTs in mice could induce an early onset and persistence of pulmonary fibrosis and pulmonary inflammation (Porter et al., 2010; Muller et al., 2005). CNTs in the alveoli could cause a burden to the macrophage, and the CNTs could migrate into the intrapleural space (Mercer et al., 2010) which, by inference, might induce certain asbestos-associated lung disease such as lung cancer and pleural mesothelioma. Based on these, the risk of exposure to CNT aerosols should be considered as a serious occupational health issue in the current nanotechnology era. The investigation of the deposition of CNTs in the human airways is therefore extremely essential for the study of CNT related lung diseases.

However, due to the fact that the dimension of the CNTs is extremely small, it is very difficult to apply the conventional fiber airway replica deposition method (Sussman et al., 1991; Su and Cheng, 2009) to CNTs for acquiring airway deposition data. The procedure of the conventional fiber airway replica deposition method involves recovering the deposited fibers from the human airway replica by flushing the airway replica after the deposition experiment and then inspecting the collected fiber samples under an optical microscope to count and measure the fiber number and dimensions. This deposition method requires the test fibers to generally maintain their original shape after being washing out from the airway replica. Also, the test fibers must be large enough to be examined under an optical microscope and to be easily differentiated from other impurities in the same field of view. However, these requirements are not feasible for CNTs, since the CNTs morphology might deform after liquid flushing, and one has to use an electrical microscope in order to unambiguously determine singular or agglomerate CNTs. Thus, the conventional fiber deposition method with using human airway replica is only suitable for fiber aerosols in the micro-scale, but not practical for CNTs or nanoparticles in the nano-scale. As a result, to date, no CNT deposition study has been carried out using a human airway replica because of the lack of the adequate experimental method. Available lung deposition data on aerosols in the nano-scale in the literature were all conducted with radioactive materials, which have to deal with generating aqueous radioactive spherical particles and rely on the assistance of a gamma counter for determining the deposition fraction (Cohen et al., 1990; Smith et al., 2001). However, to apply the radioactive-based airway deposition experiment on CNTs is considered difficult technically. Thus, there is a need to find an appropriate airway replica deposition method to investigate the deposition of CNTs in the human respiratory tract.

With this in mind, the purpose of this study was to adopt an innovative experimental approach to conduct CNT airway deposition studies to obtain some original CNT airway deposition data. In this research, two different CNT materials were aerosolized, size classified, and then delivered into a human respiratory tract replica to acquire deposition data. It is believed that the experimental data acquired by this experimental approach should well represent the CNT deposition information in the human airway. The data obtained from this research will also be valuable for assessing the risk of the worker exposure to CNTs in related occupational settings, and this can be used for verifying new numerical models developed for CNT lung dosimetry estimation.

2. Method

2.1. Human respiratory tract replica

In this research, the airway deposition experiments were conducted by using a realistic human respiratory tract replica made from a cadaver (Cheng et al., 1997; Su and Cheng, 2006). This human airway replica consists of an oral cavity, pharynx, larynx, and tracheobronchial airways down to part of the 4th lung generation. The material used for making the airway replica was conductive silicone rubber (KE-4576, Shin-Etsu Chemical Co., Ltd., Tokyo, Japan) for the purpose of preventing electrostatic effect on the deposition study. Figure 1 illustrates the airway structure of the human respiratory tract replica used in this research. Before conducting the airway deposition experiment, a thin layer of silicon oil (550 Fluid, Dow Corning Co., Midland, MI) was applied to the inside surface of the replica (dripped overnight) to simulate the wet surface nature (mucous layer) in the real human airway. This human respiratory tract replica has been used in many aerosol airway deposition studies with spherical particles or fiber aerosols in our laboratory (Cheng et al., 1999; Zhou and Cheng, 2005; Su and Cheng, 2006, 2009), and deposition results obtained showed that this airway replica is able to provide reliable experimental data for human airway deposition study. Moreover, the airway structure and dimension of this human respiratory tract replica has been well studied and defined (Zhou et al., 2008), which enables the researcher to well elucidate the deposition data acquired.

2.2. CNT materials, aerosolization, and classification

Two CNT materials, stacked-cup carbon nanotubes (SCCNT) and single-walled carbon nanotubes (SWCNT) were employed in this research for the airway deposition study. The SCCNT material (Shenzhen Nanotech Co., Shenzhen, China) was engineered in high yield from a proprietary chemical vapor deposition process, and it has more than 95% purity with tube diameters around 10–20 nm and tube length about 5–15 μm before aerosolization. The SWCNT material (SWeNT®

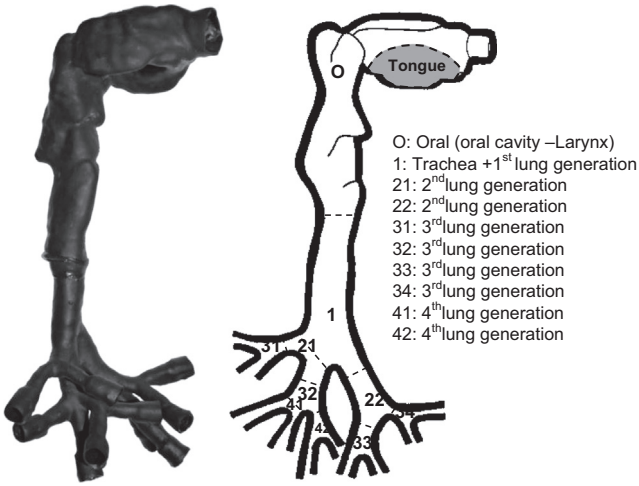

Fig. 1. The airway structure of the human respiratory tract replica.

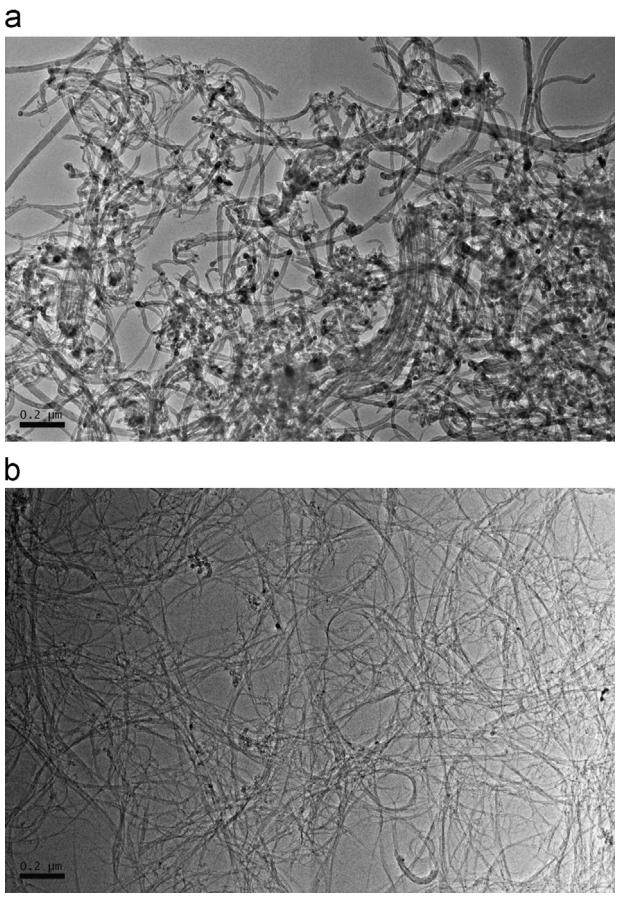

Fig. 2. CNT materials used in this deposition study: (a) stacked-cup carbon nanotubes (SCCNT) and (b) single-walled carbon nanotubes (SWCNT).

SG76, Southwest NanoTechnologies, Norman, OK) has a tube diameter of 0.93 ± 0.27 nm with more than 90% carbon content by weight. This SWCNT material contains a high length-to-diameter aspect ratio (> 1000), which indicates that this SWCNT material has extremely elongated tube length. Figure 2 shows the morphology of the SCCNT and SWCNT bulk materials used in this research.

To generate CNT aerosols for the airway deposition study, a medical nebulizer (Up-Mist, Hospitak Inc., Farmingdale, NY) was used to aerosolize the CNT materials. For preparing CNT aqueous suspension for nebulization, each CNT bulk material

was added into optima® grade Isopropanol (Fisher Scientific, Pittsburgh, PA) individually and treated with an ultrasonicator for more than 24 h to break agglomerate. In the CNT aerosol generation system, there were three drying columns to ensure the isopropanol mist generated would evaporate fast and completely with only CNT aerosols remaining in the air for the deposition study. In the last drying column, a Kr^{85} radioactive neutralizer was placed inside to discharge the CNT aerosols passing by. The charge neutralized CNTs were then delivered into a differential mobility analyzer (DMA, Model 3071A, TSI Inc., Shoreview, MN) for size classification since the deposition experiment was designed to be conducted with size classified CNT aerosols in this research. The principle of the DMA is to use the balance between the electrostatic force and the air drag force acting on aerosols to size classify polydisperse aerosols into monodisperse aerosols based on their electrical mobility diameter (d_B). The preselected classification diameters for the CNTs were 51, 101, and 215 nm. Based on these designated classification diameters, parameters were set on the DMA to classify the CNT aerosols accordingly. To make certain the size classified CNTs had the designated classification diameter, a sequential mobility particle sizer (SMPS, GRIMM Aerosol Technik GmbH & Co., Germany) was connected to the outlet of the DMA for monitoring the size distribution of the classified CNTs. Figure 3 shows the main experimental setup for generating, size classifying, and characterizing the CNT aerosols in this research. By using the SMPS together with adjusting the DMA parameters, a desired concentration peak of size classified CNTs could be shown on the SMPS right at the channel corresponding to the designated classification diameter. Figure 4 demonstrates examples of the size classified CNT aerosols measured by the SMPS. In this research, samples of size classified CNT aerosols were also collected on TEM grids for morphology analysis. The CNT sample collections were carried out by using a point-to-plane electrostatic precipitator (In-Tox Products, Albuquerque, NM), and the CNT morphology analysis was conducted by a transmission electron microscope (JEOL 2010, JEOL Ltd., Tokyo, Japan). Pictures of CNT aerosols were taken for each classification diameter and material while conducting the TEM morphology analysis.

To study the aerodynamic diameters (d_{ae}) of the size classified CNTs, the size classified CNTs were also delivered to an aerosol particle mass analyzer (APM, Kanomax USA, Inc., Andover, NJ). The main body of the APM consists of two wired co-axis metal cylinders. The principle of the APM is to utilize the balance between the electrostatic force (by varying the cylinder voltage) and centrifugal force (by varying the cylinder rpm) acting on the aerosol of interest passing the APM to acquire associated particle mass information. By operating the APM with the DMA to form a DMA-APM tandem setup, together with using PSL particles as reference, the aerodynamic diameter of the size classified CNTs can then be estimated. It is worth noting that the experimental setup, procedure, and calculation of the DMA-APM tandem technique carried out in this research has already been well established and applied in many studies to investigate the aerodynamic diameters of nanoparticles and nanofibers (McMurry et al., 2002; Park et al., 2003; Ku et al., 2006).

2.3. Estimation of CNT airway deposition

The CNT airway deposition experiment was designed to be done by delivering size classified CNT aerosols into human respiratory tract replicas. Then, by measuring the ratios of the CNT concentration at different lung tube outlets to the oral inlet, the deposition fraction of CNT aerosols in each airway section of the respiratory tract replica can be estimated. Figure 5

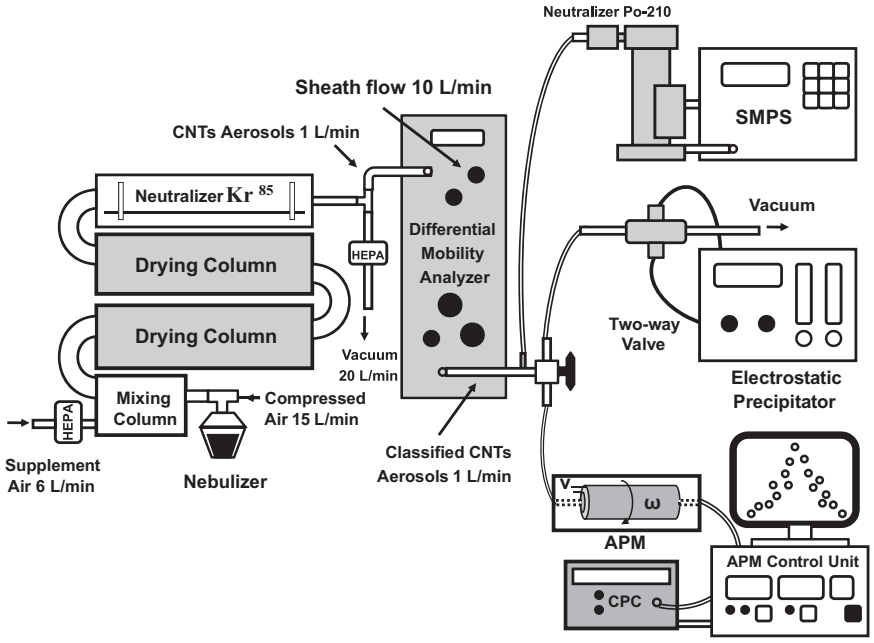

Fig. 3. The experimental setup for the CNT aerosols generation, size classification, and characterization.

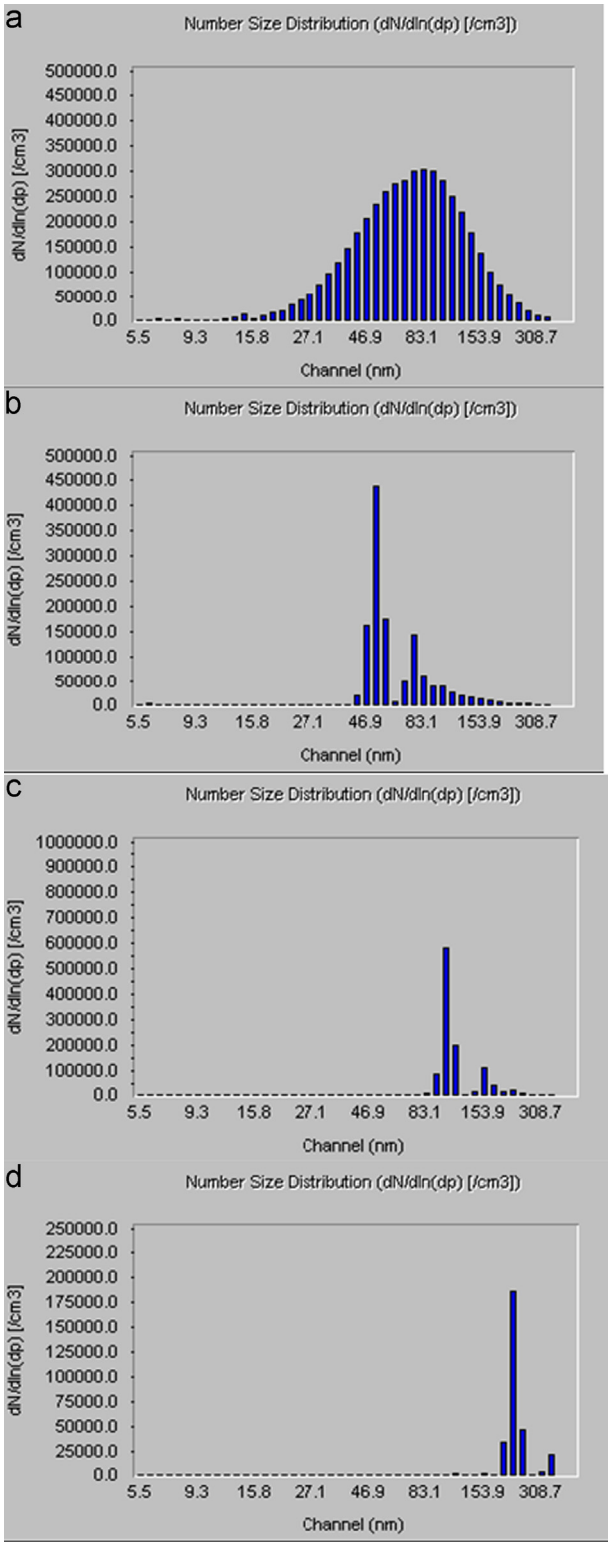

Fig. 4. The size distribution of the classified CNTs: (a) before size classification, (b) after 51 nm size classification, (c) after 101 nm size classification, and (d) after 215 nm size classification.

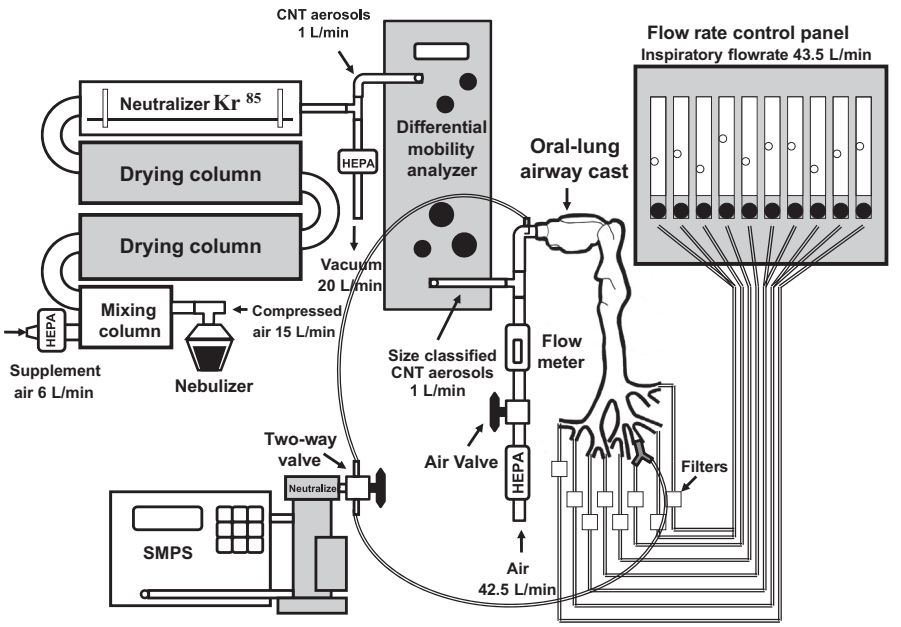

Fig. 5. The experimental setup of the airway deposition study using size classified CNTs.

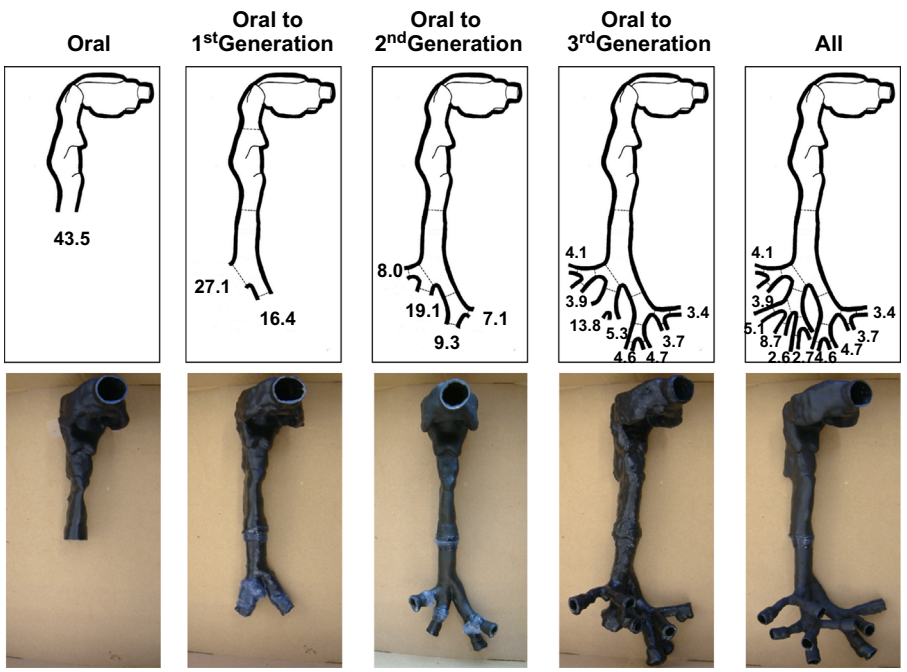

Fig. 6. The schematic and physical model of the airway replicas used in this research (also shown are associated lung tube flow rates).

describes the experimental setup used in this research. Since the CNT concentration measurement had to be taken at two different locations of the airway replica (lung tube outlet and oral inlet) for obtaining concentration ratio, a two-way valve was installed at the SMPS inlet for facilitating the switch of the measurement taking. An inspiratory flow rate of 43.5 L/min was used for the deposition study. This flow rate represents the inhalation flow rate of a worker having a heavy workload (NCRP, 1997), and this has been used in the past for conducting fiber lung deposition studies in our laboratory. The flow rate distribution in the airway replica under this inspiratory flow rate has been well defined.

The theory to estimate the deposition fraction of size classified CNTs in a specific lung bifurcation of the airway replica is as follows: based on the principle of mass conservation, the deposition of size classified CNTs within a lung bifurcation can

be determined by the decrease of the CNT number after passing the lung bifurcation, which can be expressed as

$$D_{lung} = N_{enter} - N_{exit}, \tag{1}$$

where D_{lung} is the number of CNTs deposited in the lung bifurcation, N_{enter} is the number of CNTs that entered the lung bifurcation, and N_{exit} is the number of the CNTs that exited the lung bifurcation. A lung bifurcation has one parent tube and two daughter tubes, and the number of CNTs in each lung tube can be calculated by related CNT concentration and the flow rate. Therefore, Eq. (1) can be rewritten as

$$D_{lung} = Q_p C_p - (Q_{d1} C_{d1} + Q_{d2} C_{d2}), \tag{2}$$

where Q_p is the air flow rate entering the parent tube of the lung bifurcation, C_p is the CNT concentration measured at the parent tube of the lung bifurcation, Q_{d1} and Q_{d2} are the air flow rates in the two daughter tubes of the lung bifurcation, and C_{d1} and C_{d2} are the CNT concentration measured at the two daughter tubes of the lung bifurcation. By dividing Eq. (2) with the total number of CNTs that entered the entire airway replica, $Q_o C_o$, the deposition fraction of the CNTs in the specific lung

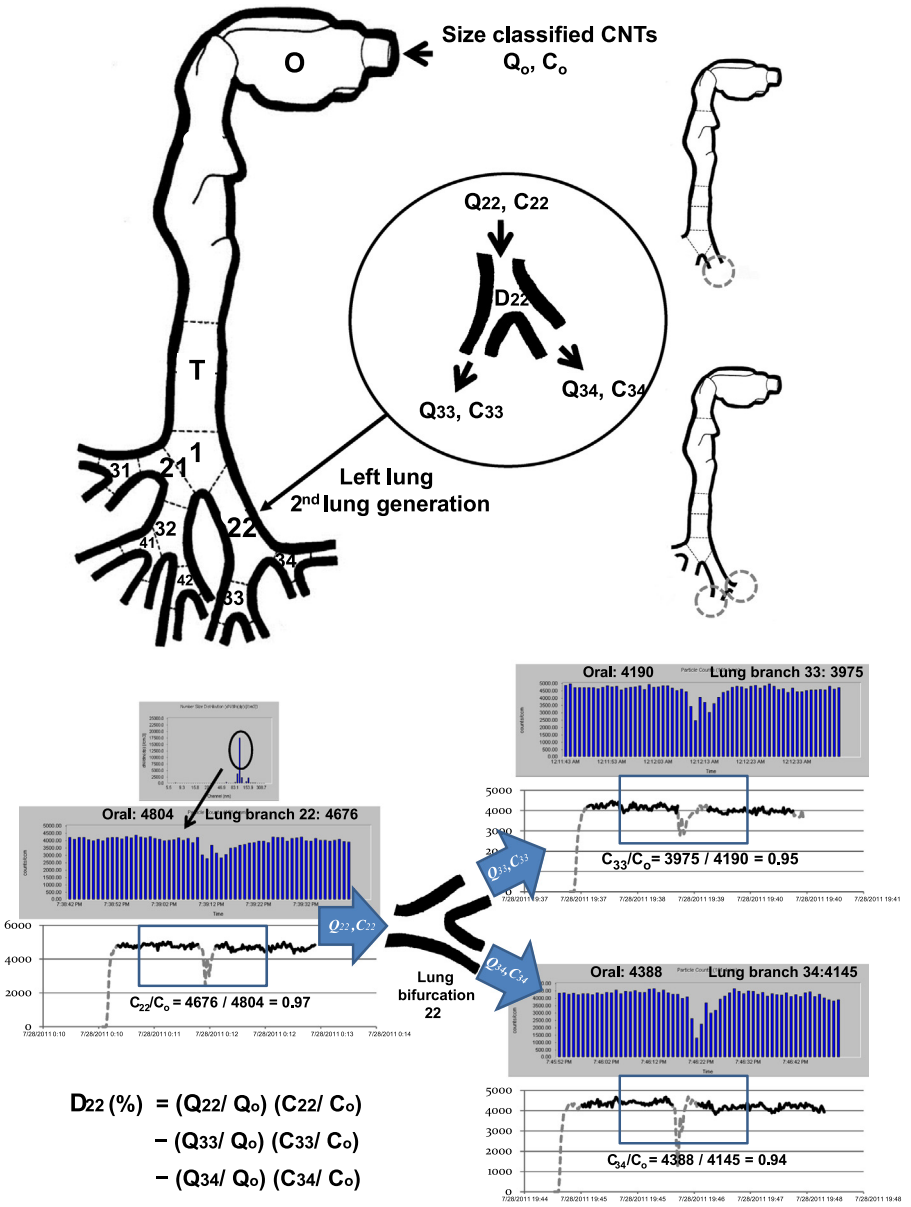

Fig. 7. The procedure to estimate the deposition fraction of size classified CNTs in a lung bifurcation.

bifurcation (the percentage of the total CNT amount that entered the airway replica), $D_{lung}(\%)$, can be calculated as

$$D_{lung}(\%) = \frac{D_{lung}}{Q_o C_o} = \frac{Q_p}{Q_o}\frac{C_p}{C_o} - \frac{Q_{d1}}{Q_o}\frac{C_{d1}}{C_o} - \frac{Q_{d2}}{Q_o}\frac{C_{d2}}{C_o}, \tag{3}$$

where Q_o is the total flow rate entering the entire airway replica (43.5 L/min in this research) and C_o is the CNT concentration measured at the oral inlet. For Eq. (3), given that the flow rate distribution in the airway replica is already defined (which means Q_o, Q_p, Q_{d1} and Q_{d2} are already known), only the CNT concentration ratios C_p/C_o, C_{d1}/C_o, and C_{d2}/C_o need to be measured to obtain the $D_{lung}(\%)$. Based on Eq. (3) and according to the human respiratory tract replica used in this research with 10 airway sections from the oral airway down to part of the 4th lung generation, only 19 different locations on the airway replica need the concentration ratio to be measured for obtaining a completed fractional deposition map. It is because a concentration ratio obtained from a certain lung tube could be used as the daughter tube ratio for a certain lung bifurcation. At the same time, it also could be used as the parent tube ratio for the consecutive lung bifurcation. To assist the concentration ratio measurement, several identical human respiratory tract replicas were modified by the lung generation based on the airway physiology structure. Figure 6 demonstrates all airway replicas used in this research with flow rates indicated at corresponding lung tubes. Once all needed CNT concentration ratios are measured and available, the CNT deposition fraction in each lung bifurcation in the airway replica can be estimated, and a complete CNT airway fractional deposition map can then be constructed.

As shown in Fig. 4 and mentioned previously, the size classified CNTs presents an apparent peak concentration right at the SMPS channel bar corresponding to the designated classification diameter. To make full use of this peak concentration, only the single channel bar showing the peak concentration was used when conducting the deposition experiment in this research. All other channels were turned off for the purpose of making the deposition experiment focus solely on the CNTs with the designated classification diameter. Figure 7 shows an illustration of the experimental procedure for estimating the CNT deposition fraction in the 2nd lung generation of the left lung (lung bifurcation 22). As can be seen, the SMPS measured the concentration of the size classified CNT in every second, and the abrupt concentration change during the measurement indicates the measurement taking was switched from the oral inlet to the lung tube outlet. The SMPS instrument raw data could be exported to MS Excel for estimating the average concentration at the oral inlet and the lung tube outlet, and then the CNT concentration ratio needed for calculating the deposition fraction in Eq. (3) could be acquired. In this research, the concentration ratio at each lung tube was measured at least three times for obtaining statistically meaningful data.

In this research, since the size classified CNT aerosols used in this deposition study were all in the submicron scale, CNT loss due to diffusion deposition on the wall of the tubing, valve, and connectors while transiting to the SMPS for measurement is a concern. To more accurately estimate the CNT airway deposition, this diffusion loss of the experimental setup has to be studied. For this reason, experiments were carried out to investigate the particle delivery efficiency correction factor, F, for the experimental setup used in this research. The particle delivery efficiency correction factor is defined as the ratio of the particle concentration measured at the oral airway connector (in) to the lung tube connector (out), $F = C_{in}/C_{out}$, while there is no airway replica installed in the experimental setup. The concentration ratios measured under this condition represent the inherent particle loss in the tubing system of the experimental setup. Figure 8 shows the

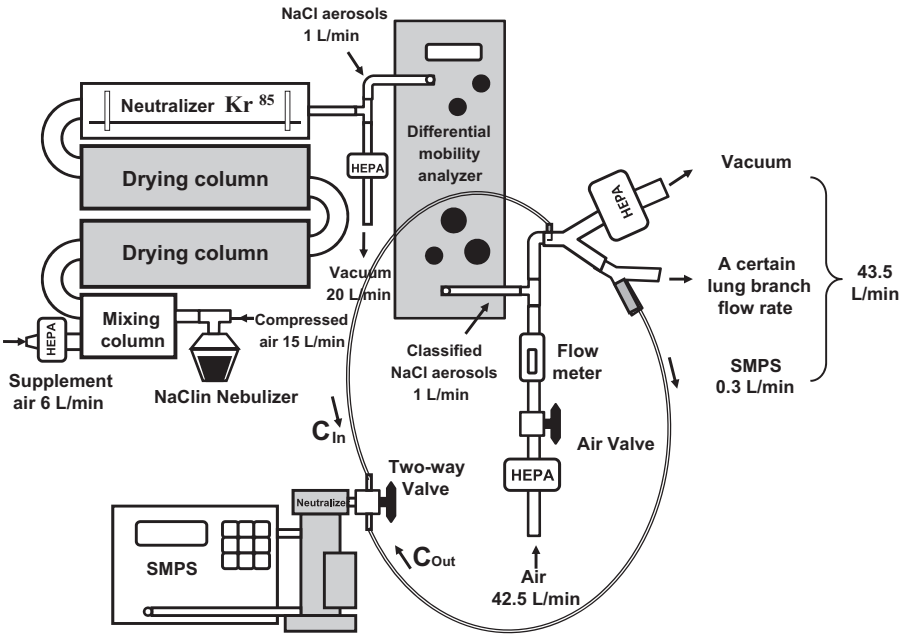

Fig. 8. The experimental setup for particle delivery efficiency correction factor investigation.

setup for the particle delivery efficiency correction factor investigation. The particle delivery efficiency correction factors obtained were then used to correct/adjust the concentration ratios measured in the real CNT deposition experiment when an airway replica is in use. In other words: *True concentration ratio* = *Particle delivery efficiency correction factor* × *Measured concentration ratio*. In this study, the investigation of the particle delivery efficiency correction factor was conducted by size classified sodium chloride (NaCl) particles with the same experimental setup used for the real CNT deposition study, including the nebulizer generation system, DMA, and SMPS. Besides, the particle delivery efficiency correction factor investigation was carried out with all experimental conditions used in the real CNT deposition study (combined with three classification diameters and different lung tube flow rates). Moreover, for the purpose of data comparison in this research, airway deposition studies were conducted with the size classified NaCl aerosols as well by the same experimental approach

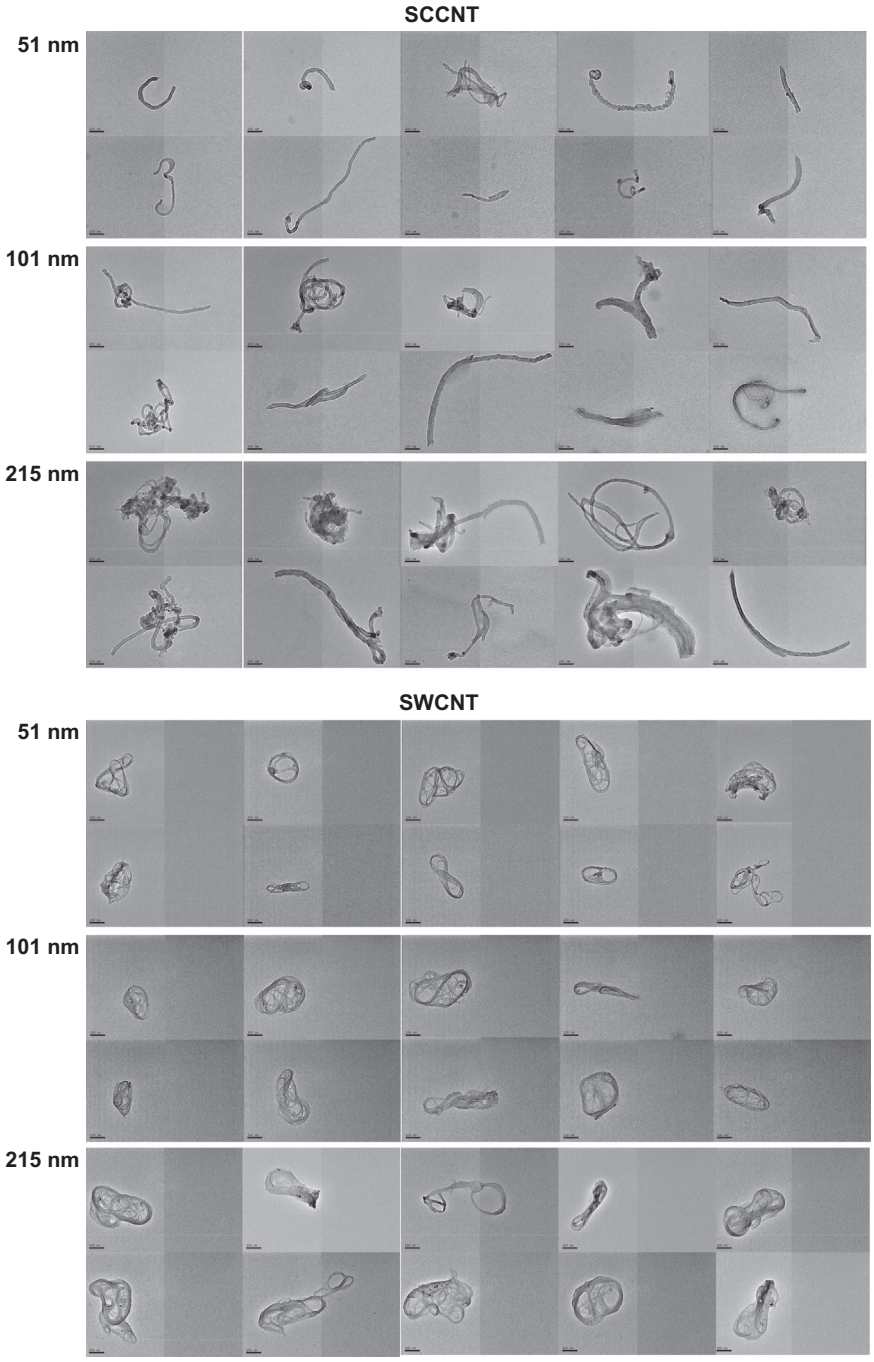

Fig. 9. The morphology of the size classified SCCNTs and SWCNTs (reference bars in each subpicture represent 100 nm).

described above. The size classified NaCl aerosols could represent some general compact particles possessing the same electrical mobility diameter, but having quite distinct particle morphology from the CNT aerosols. Therefore, the deposition results obtained by NaCl particles could provide useful insight and information about the similarity or discrepancy of aerosol airway deposition between compact particles and CNTs.

3. Results

Based on the generation, classification, characterization, and deposition methods described above, data were acquired for each experiment accordingly. Figure 9 demonstrates examples of size classified SCCNT and SWCNT aerosols collected by the electrostatic precipitator. It can be seen that the morphology of the SCCNT and SWCNT aerosols were noticeably distinct. Most of the size classified SCCNT aerosols still show a fiber-like morphology to a certain extent. On the other hand, all of the size classified SWCNT aerosols were found to be similar to twisted rubber bands. Table 1 presents the aerodynamic diameters of the size classified SCCNTs and SWCNTs acquired from the DMA-APM tandem study. It can be seen that the d_{ae} of the size classified CNT aerosols were generally close, but a little less than their d_B (classification diameter). Figure 10 shows the results obtained from the particle delivery efficiency correction factor investigation. Based on these particle delivery efficiency correction factor data, regression lines were fitted for each classification diameter (linear relationship was assumed), and the equations obtained are also shown in Fig. 10. Figure 11 shows the fractional deposition map of size classified CNTs in the human respiratory tract replica for SCCNTs and SWCNTs. It can be seen that the CNT deposition fractions were generally less than 5% in each airway section in the airway replica. Figure 12 shows the CNT deposition efficiency in the human oral airway as a function of impaction parameter $d_{ae}^2 Q$. The impaction parameter is a common physical property used for presenting aerosol deposition data in irregular or complicated human airways such as oral and nasal airways. The deposition efficiency is defined as the ratio of aerosols that deposited within a certain airway section to the total aerosols that entered the airway section. The deposition efficiency for an airway section or a lung bifurcation could be calculated by the deposition fraction data acquired above. Figures 13–15 show the deposition efficiency of size classified CNTs in the tracheobronchial airways from the 1st to the 3rd lung generation. The deposition efficiency data were plotted as a function of the Stokes number, which is a dimensionless physical property usually used for presenting aerosol deposition data in lung airways. The Stokes number for a lung bifurcation is expressed as

$$\mathrm{Stk} = \frac{\rho_o {d_{ae}}^2 U_s}{18\eta D}, \tag{4}$$

Table 1
The aerodynamic diameters of the size classified SCCNTs and SWCNTs acquired from the DMA-APM tandem study.

CNT material	Electrical mobility diameter d_B (nm)	Aerodynamic diameter d_{ae} (nm)
SCCNT	51	46.8 ± 0.1
	101	88.8 ± 0.2
	215	183.8 ± 1.6
SWCNT	51	47.2 ± 0.2
	101	94.0 ± 0.3
	215	194.4 ± 0.9

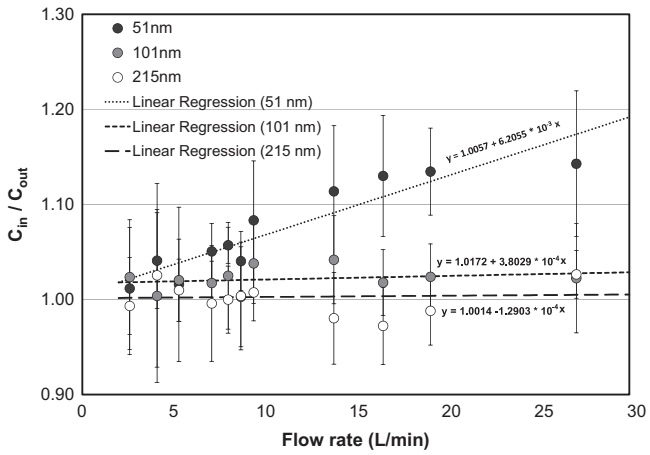

Fig. 10. The particle delivery efficiency correction factors obtained from the particle delivery efficiency correction factor investigation.

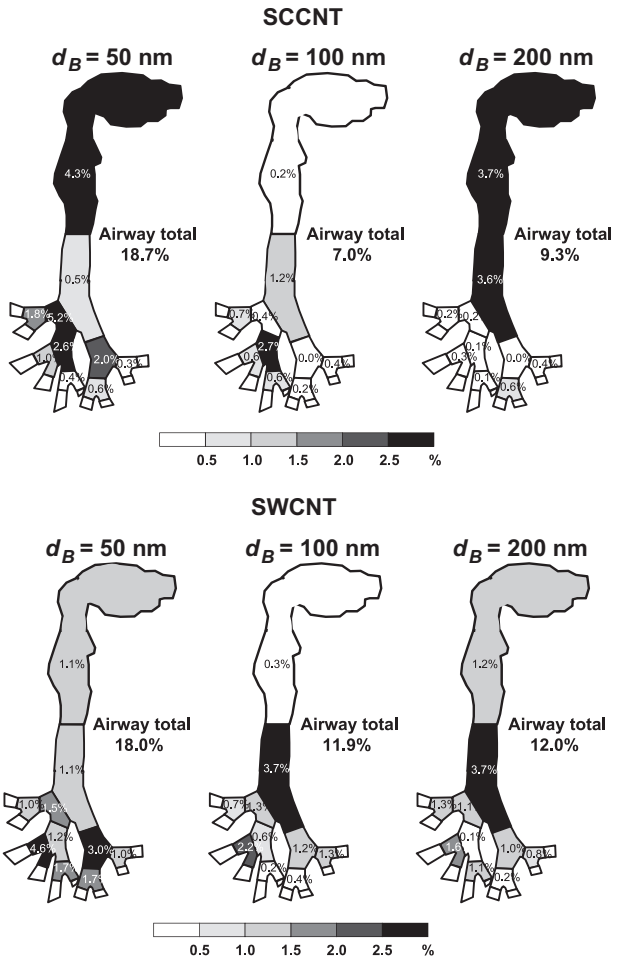

Fig. 11. CNT fractional deposition map in the human respiratory tract replica.

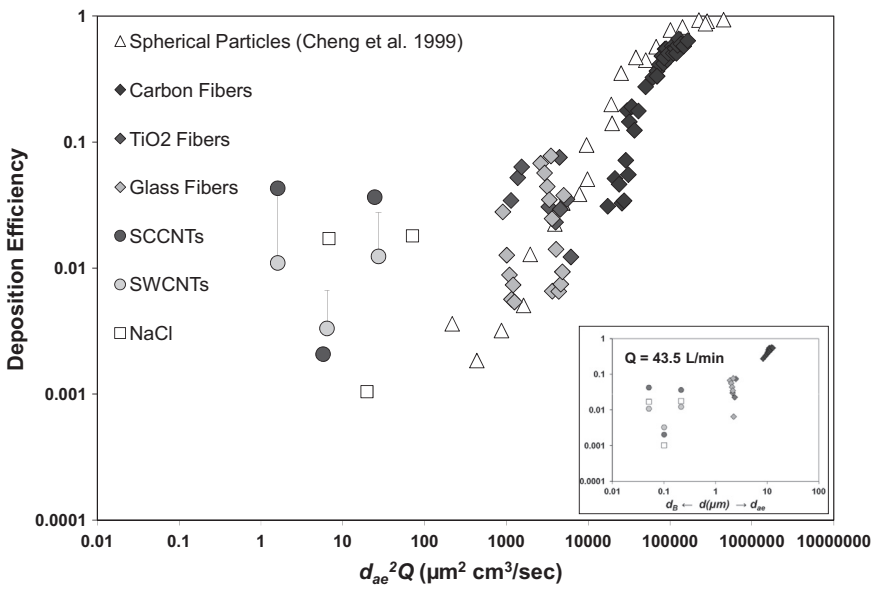

Fig. 12. The deposition efficiency of CNTs in the human oral airway as a function of impaction parameter.

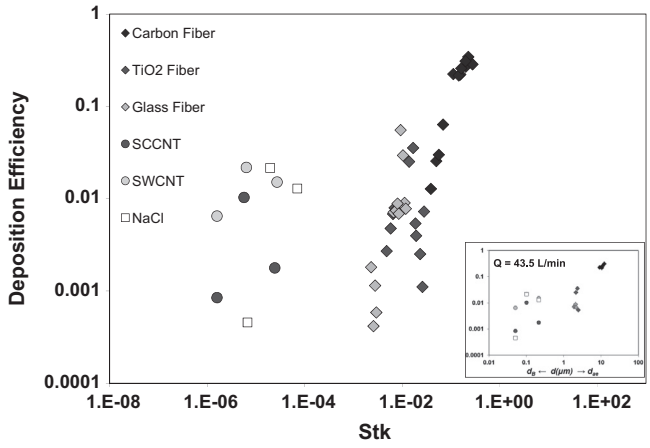

Fig. 13. The deposition efficiency of CNTs in the 1st lung generation as a function of Stokes number.

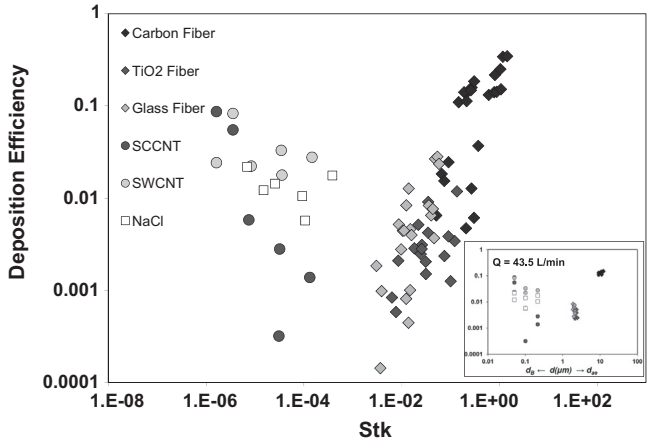

Fig. 14. The deposition efficiency of CNTs in the 2nd lung generation as a function of Stokes number.

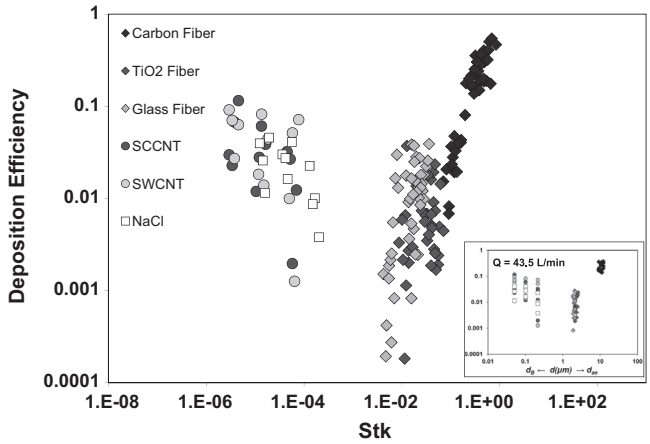

Fig. 15. The deposition efficiency of CNTs in the 3rd lung generation as a function of Stokes number.

where ρ_o is the density of water, U_s is the mean air velocity in the parent tube of the lung bifurcation, η is the air viscosity, and D is the mean diameter of the parent tube of the lung bifurcation. It is worth noting that the d_{ae} needed for calculating the impaction parameter and Stk for size classified CNTs were all provided from Table 1. Also shown in Figs. 12–15 are compact particle data obtained from the size classified NaCl in this research, and fiber data acquired previously from our laboratory with using the same human respiratory tract replica (Su and Cheng, 2009). The inserted graphs in Figs. 12–15

show all deposition data obtained with inspiratory flow rate of 43.5 L/min plotted as a function of the particle diameter for the purpose of reference.

4. Discussion

As can be seen in Fig. 4, the CNT aerosols could be ideally size classified by their d_B with a DMA, which can be seen evidently as the concentration peaks shown at the corresponding channels (51, 101, and 215 nm) by the SMPS. Although minor peaks were also shown on the SMPS, especially for the 51 nm, it could be safe to state that the majority of the size classified CNTs all have a d_B the same as the designated classification diameter. Nevertheless, the experimental method designed in this research was to use only one SMPS channel for the deposition study. Therefore, the influence of the minor peaks on the final deposition result was limited, and focus was made solely on the designated classification diameter. On the other hand, it is surprising to learn from Fig. 9 that, even though the CNT aerosols have been size classified, they still could be in a variety of complicated shapes. The morphology of size classified SCCNTs showed a curved, rope-like, circular loop, and bird nest-like single or aggregated morphology. In contrast, the size classified SWCNTs resembled a twisted rubber band and open cage-like structure consisting of very thin nanotubes. For both size classified SCCNTs and SWCNTs, they displayed a common characteristic in that their physical dimensions were generally much larger than their d_B (the reference bar in each CNT subpicture indicates 100 nm). This result implies that both SCCNT and SWCNT aerosols are constructed by loose nanotubes with considerable empty space. Therefore, even though the dimensions of CNT aerosol were much larger than their designated classification diameters, their d_B are compromised by their limited mass contained within due to the empty space (effective density reduced). This statement is in agreement with what was found in the DMA-APM tandem study in this research, which also showed the d_{ae} obtained from the size classified CNT aerosols were generally less than their d_B, and the larger the CNT aerosol, the less d_{ae} than d_B. Some published research also demonstrated a similar result for other types of CNT materials, as well as aggregated nanoparticles, by using the DMA-APM tandem technique (McMurry et al., 2002; Park et al., 2003; Ku et al., 2006).

As mentioned in the previous section, equations were obtained from the linear regression analysis for the particle delivery efficiency correction factors found in this research. With these equations, particle delivery efficiency correction factors could be calculated as a function of the lung tube flow rate for each designated classification diameter in order to correct/adjust the CNT concentration ratio measured under the same experimental conditions (lung tube flow rate and classification diameter). Figure 10 shows that the particle delivery efficiency correction factors were close to 1.0 in general for both 101 and 215 nm classification diameters for all lung tube flow rates used, which implies that the diffusion loss in the tubing system of the experimental setup was minimal for aerosols with these two classification diameters. However, for the 51 nm classification diameter, the particle delivery efficiency correction factors were found to be significant and increased as the flow rate increased. Most of the particle delivery efficiency correction factors calculated showed larger than 1.05. This result implies that the aerosol diffusion loss in the tubing system of the experimental setup is substantial for particles with small d_B such as 51 nm. Therefore, with the particle delivery efficiency correction factor equation available and by applying the calculated particle delivery efficiency correction factors to adjust the associated measured CNT concentration ratios, it would be able to provide a more precise estimation for the deposition of CNT in the human airway.

The fractional deposition map shown in Fig. 11 indicates that the deposition of SCCNTs and SWCNTs in the airway replica was generally small and expressed no appreciable difference between CNT materials. The deposition fractions obtained in each airway section were all smaller than 5%, and generally there was no apparent deposition pattern and trend shown by different classification diameters used. Upon closer examination, only the 51 nm CNTs showed some slightly higher deposition fractions in the tracheobronchial airways than the other two classification diameters, but it was not very significant. The overall deposition fraction in the entire airway replica was around 7–19% for SCCNTs and 12–18% for SWCNTs. This result implies that more than 80% of the SCCNTs and SWCNTs inhaled into the oral airway with a d_B within the range studied in this research would easily transit to lower than the 4th lung generation, where possible adverse respiratory health effects could develop. Some published studies showed similar results that ultrafine particles with diameters similar to the designated classification diameters in our research presented low deposition in the tracheobronchial airways (Cohen et al., 1990; Smith et al., 2001). On the other hand, in Figs. 12–15 the deposition efficiencies of CNTs were found generally to be less than 0.1, and the data points of SCCNTs and SWCNTs were scattered and showed no significant discrepancy with each other. When comparing the deposition efficiency of CNTs together with other fiber data and compact particles in Figs. 12–15, it can be seen that each data group seems to be able to connect with each other and form a letter “U” like data trend. This U-type deposition data trend indicates that, for large fiber aerosols such as carbon fibers, their airway deposition efficiency increases as their inertia is increasing (aerosol inertia is shown in the form of impaction parameter and Stk); however, for small fiber aerosols like CNTs, their deposition efficiency increases as their inertia is decreasing. This result indicates that the deposition mechanism is discrepant between carbon fibers and CNTs. Also, it can be seen in Figs. 12–15 that the deposition efficiencies of CNTs were comparable to those of compact NaCl particles in all airways. This result implies that, for the size classified CNTs studied in this research, once the CNT has a similar inertia (Stk) as a compact particle (even though their morphologies are complicated and their physical dimensions are much larger than their designated classification diameter), the CNT will then behave similarly to a compact particle and have the same deposition mechanism. This will result in a comparable deposition efficiency in the human upper airways.

5. Conclusion

In this research, CNT airway deposition studies were successfully conducted by adopting an innovative experimental approach using DMA size classified SCCNT and SWCNT aerosols and a human respiratory tract replica. By measuring the CNT concentration ratio at each lung tube of the modified human airway replicas together with the information of the flow rate distribution in the airway replica, the CNT deposition fraction and deposition efficiency in each airway section of the airway replica can be effectively estimated. The experimental results obtained showed that the CNT deposition fractions from the oral to part of the 4th lung generation were commonly less than 5%. Moreover, the CNT deposition efficiency in the oral airway and tracheobronchial airways were lower than 0.1 in general. These results imply that a considerable amount of the CNTs inhaled into the human respiratory tract through the oral airway could easily transit down to the lower tracheobronchial airways, where adverse biological response could be induced. The experimental approach used in this deposition study is believed to be a useful experimental method to apply on other types of CNTs or nanomaterials for airway deposition studies.

Acknowledgment

The authors are grateful to Eileen Kuempel and Pramod Kulkarni at NIOSH for developing the concept of this research project and to Bean Chen, Bon-Ki Ku and Bahman Asgharian for useful discussion on related subjects. This project was sponsored by NIOSH contract 254-2010-M-36304, 214-2012-M-52048 and research grant R01OH010062.

References

Chen, B.T., Schwegler-Berry, D., McKinney, W., Stone, S., Cumpston, J.L., Friend, S., Porter, D.W., Castranova, V., & Frazer, G. (2012). Multi-walled carbon nanotubes: sampling criteria and aerosol characterization. *Inhalation Toxicology*, *24*, 798–820.

Cheng, Y.S., Smith, S.M., & Yeh, H.C. (1997). Deposition of ultrafine particles in human tracheobronchial airways. *The Annals of Occupational Hygiene*, *41*(S1), 714–718.

Cheng, Y.S., Zhou, Y., & Chen, B.T. (1999). Particle deposition in a cast of human oral airways. *Aerosol Science Technology*, *31*, 286–300.

Cohen, B.S., Sussman, R.G., & Lippmann, M. (1990). Ultrafine particle deposition in a human tracheobronchial cast. *Aerosol Science and Technology*, *12*, 1082–1091.

Dahm, M.M., Evans, D.E., Schubauer-Berigan, M.K., Birch, M.E., & Fernback, J.E. (2012). Occupational exposure assessment in carbon nanotube and nanofiber primary and secondary manufacturers. *Annual Occupational Hygiene*, *56*(3), 542–556.

De Volder, M.F.L., Tawfick, S.H., Baughman, R.H., & Hart, A.J. (2013). Carbon nanotubes: present and future commercial applications. *Science*, *339*, 535–539.

Endo, M., Strano, M.S., & Ajayan, P.M. (2008). Potential applications of carbon nanotubes. In A. Jorio, G. Dresselhaus, & M.S. Dresselhaus (Eds.), *Carbon Nanotubes*. Springer: New York, pp. 13–61.

Ku, B.K., Emery, M.S., Maynard, A.D., Stolzenburg, M.R., & McMurry, P.H. (2006). in situ structure characterization of airborne carbon nanofibers by a tandem mobility-mass analysis. *Nanotechnology*, *16*, 3613–3621.

McMurry, P.H., Wang, X., Park, K., & Ehara, K. (2002). The relationship between mass and mobility for atmospheric particles: a new technique for measuring particle density. *Aerosol Science and Technology*, *36*, 227–238.

Mercer, R.R., Hubbs, A.F., Scabilloni, J.F., Wang, L., Battelli, L.A., Schwegler-Berry, D., Castranova, V., & Porter, D.W. (2010). Distribution and persistence of pleural penetrations by multi-walled carbon nanotubes. *Particle and Fibre Toxicology*, *7*(28), 1–11.

Muller, J., Huaux, F., Moreau, N., Misson, P., Heilier, J.F., Delos, M., Arras, M., Fonseca, A., Nagy, J.B., & Lison, D. (2005). Respiratory toxicity of multi-wall carbon nanotubes. *Toxicology and Applied Pharmacology*, *207*(3), 221–231.

National Institute for Occupational Safety and Health (NIOSH) (2013). Current intelligence bulletin: occupational exposure to carbon nanotubes and nanofibers. DHHS (NIOSH) Publication No. 2013-145.

NCRP (1997). National council on radiation protection and measurements: deposition, retention and dosimetry of inhaled radioactive substances, NCRP Report No. 125, National Council on Radiation Protection and Measurements, Bethesda, MD.

Parish, A. (2011). *Production and applications of Carbon Nanotubes, Carbon Nanofibers, Fullerenes, Graphene and Nanodiamonds: A Global Technology Survey and Market Analysis*. Innovative Research and Products, Inc.: Stamford, CT.

Park, K., Cao, F., Kittelson, D.B., & McMurry, P.H. (2003). Relationship between particle mass and mobility for diesel exhaust particles. *Environmental Science and Technology*, *37*, 577–583.

Porter, D.W., Hubbs, A.F., Mercer, R.R., Wu, N., Wolfarth, M.G., Sriram, K., Leonard, S.S., Battelli, L., Schwegler-Berry, D., Friend, S., Andrew, M., Chen, B.T., Tsuruoka, S., Endo, M., & Castranova, V. (2010). Mouse pulmonary dose- and time course-responses induced by exposure to multi-walled carbon nanotubes. *Toxicology*, *269*, 136–147.

Smith, S., Cheng, Y.S., & Yeh, H.C. (2001). Deposition of ultrafine particle in human tracheobronchial airway of adults and children. *Aerosol Science and Technology*, *35*, 697–709.

Su, W.C., & Cheng, Y.S. (2006). Deposition of fiber in a human airway replica. *Journal of Aerosol Science*, *37*(11), 1429–1441.

Su, W.C., & Cheng, Y.S. (2009). Deposition of man-made fibers in human respiratory airway casts. *Journal of Aerosol Science*, *40*(3), 270–284.

Sussman, R.G., Cohen, B.S., & Lippmann, M. (1991). Asbestos fiber deposition in human tracheobronchial cast. I. Experimental. *Inhalation Toxicology*, *3*, 145–160.

Zhou, Y., & Cheng, Y.C. (2005). Particle deposition in a cast of human tracheobronchial airways. *Aerosol Science and Technology*, *39*, 492–500.

Zhou, Y., Su, W.C., & Cheng, Y.S. (2008). Fiber deposition in the tracheobronchial region: deposition equations. *Inhalation Toxicology*, *20*(13), 1191–1198.